Radiation and Scattering from Thin Toroidally Knotted Wires

Douglas H. Werner, *Senior Member, IEEE*

***Abstract*—The electromagnetic radiation and scattering properties of thin knotted wires are considered in this paper. A special class of knots, called torus knots, are introduced for the purpose of this investigation. The parameterizations available for torus knots are used in conjunction with Maxwell's equations to formulate useful mathematical representations for the fields radiated by these knots. These representations are then used to derive simple closed form far-field expressions for electrically small torus knots. The derivation of a new electric field integral equation (EFIE) suitable for analysis of toroidally knotted wires is also outlined in this paper. Finally, it is demonstrated that the well-known expressions for the electromagnetic fields radiated by a circular loop antenna (canonical unknot) may be obtained as degenerate forms of the more general torus knot field representations.**

***Index Terms*—Dielectric materials, electromagnetic radiation, electromagnetic scattering, inhomogeneous media, knot electrodynamics.**

I. Introduction

OVER the past 100 years, the study of knots has been primarily confined to the field of mathematics. Knot theory is a subfield of an area of mathematics known as topology, which deals with the properties of geometric objects that are preserved under deformations. A knot is defined as a closed curve in space that does not intersect itself anywhere [1]. In knot theory, there is no distinction placed on the original closed knotted curve and the deformations of that curve through space that do not allow the curve to pass through itself. All of these deformations are considered to be the same knot. In other words, they are topologically equivalent. The simplest of all possible knots is the unknotted circle or loop, which is called the unknot or trivial knot. At first glance, a tangled-up loop of string may appear to be knotted, but actually it can be untangled without cutting and gluing. In this case, the tangled-up loop of string degenerates into an unknot.

It has only been over the past few years that knots have been gaining interest outside the field of mathematics in various branches of science and engineering. For instance, applications of knot theory are emerging in such diverse fields as plasma physics, polymer science, and molecular biology. Biochemists have recently discovered that knotting exists in DNA molecules [2], [3]. Since then, synthetic chemists have been studying ways to create knotted molecules in which the type of knot would determine the properties of the molecule [1], [4]. Knots have also been considered in electrostatic and magnetostatic field theory with applications to the study of eruptive solar flares and magnetohydrostatics [5], [6].

The first application of knot theory to electrodynamics was recently reported by Manuar and Jaggard [7]. The initial investigations in [7] suggest that the handedness of knots and the degree of knottedness may be deduced from the backscatter signature of electromagnetic waves. The work reported in [7] is based on results obtained for the backscatter differential cross section of the threefold rotationally symmetric trefoil knot and its associated unknot. The trefoil knot is the name given to the simplest nontrivial knot. A trefoil knot can be constructed by tieing a piece of string in a knot and gluing the two ends of the string together. Trefoils were chosen in [7] because they posses a low knottedness and it only takes one crossing switch (cut and reattach) to transform the trefoil into its corresponding unknot. Further discussions of the scattering properties of trefoils and untrefoils may be found in [8] and [9].

One of the major drawbacks for application of knot theory to electromagnetics has been the lack of available parameterizations that can be used to mathematically describe knotted curves. This is because knots have traditionally been studied within a topological context where parameterizations for the curves are not generally required. However, in order to successfully characterize the electromagnetic radiation and scattering properties of knots using Maxwell's equations, it is advantageous to develop parameterizations which can be used to geometrically describe the curves of these knots. This paper introduces such parameterizations for a family of knots known as (p,q)-torus knots. These knots reside on the surface of a standard torus, thereby making it possible to readily obtain useful parameterizations to describe them. The well-known trefoil is one important example of a (p,q)-torus knot.

The parametric representations for the (p,q)-torus knots are presented in Section II. These parameterizations are then used in combination with Maxwell's equations to derive the vector potential and corresponding electric field expressions, which describe radiation from a (p,q)-torus knot. The derivation of an electric field integral equation (EFIE) specifically for (p,q)-torus knots is also outlined in Section II. In Section III, closed-form expressions are derived for the radiation integrals associated with electrically small (p,q)-torus knots. It is also demonstrated in Section III that the well-known expressions for the electromagnetic fields radiated by a circular loop antenna (canonical unknot) may be obtained as degenerate forms of the more general torus knot field representations derived

Manuscript received March 7, 1997; revised June 17, 1999.

The author is with the Applied Research Laboratory, The Pennsylvania State University, State College, PA 16804 USA.

Publisher Item Identifier S 0018-926X(99)07968-5.

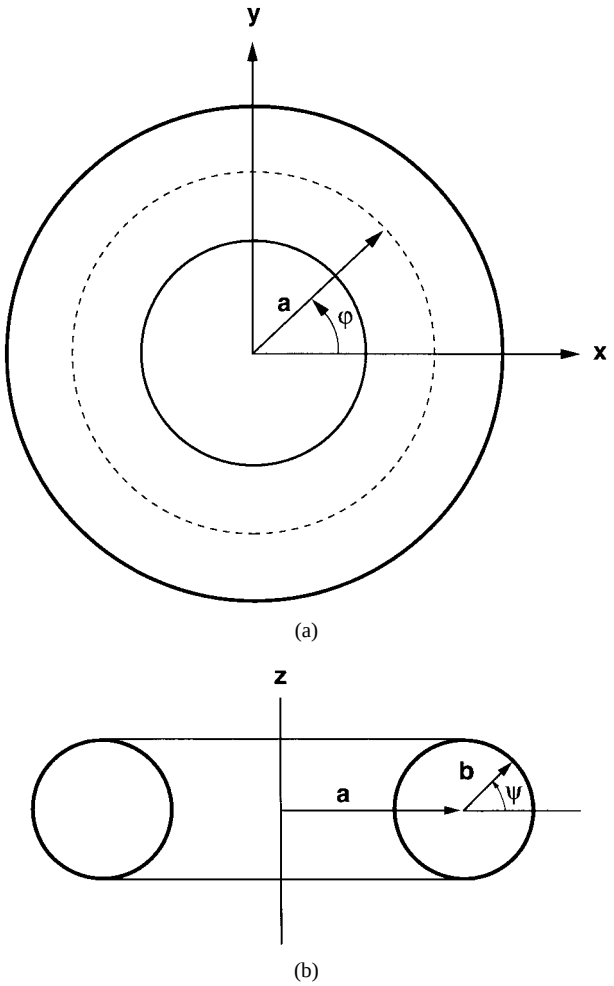

Fig. 1. Geometry of the solid torus $\mathbf{T}$. (a) The top view. (b) Side view.

in Section II. Several examples illustrating the radiation and scattering properties of various (p,q)-torus knots, including the trefoil, are presented in Section IV. These results were obtained by performing a method of moments analysis on thin knotted wires, using the parameterizations introduced to define the wire geometry.

II. Theoretical Development

A. Background

Let $\mathbf{T}$ denote the standard solid torus in R^3, which is depicted in Fig. 1. The (x,y,z) coordinates that describe this solid torus $\mathbf{T}$ are given by

$$x = (a + b\cos\psi)\cos\varphi \tag{1a}$$

$$y = (a + b\cos\psi)\sin\varphi \tag{1b}$$

$$z = b\sin\psi \tag{1c}$$

where $0 \leq \psi, \varphi \leq 2\pi$, and $0 \leq b \leq a/2$. There are two types of curves, known as meridian and longitude curves, which are commonly associated with the torus $\mathbf{T}$. A meridian curve runs once the short way around the torus, while a longitude curve runs once around the torus the long way. An example of these curves is illustrated in Fig. 2.

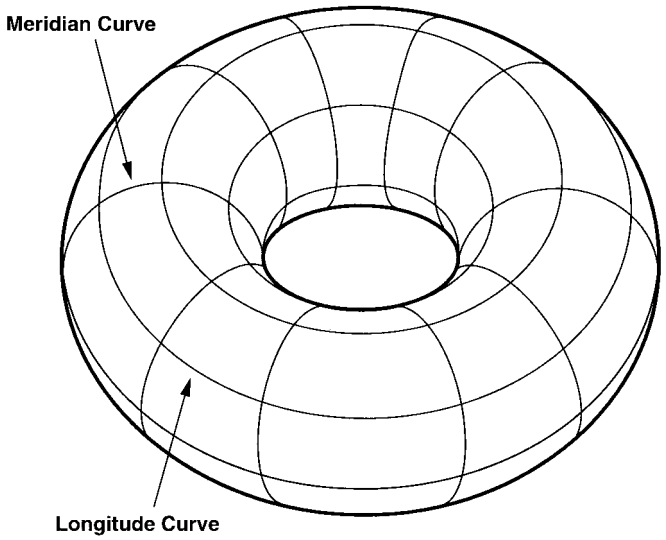

Fig. 2. Examples of meridian and longitude curves on the surface of a torus $\mathbf{T}$.

The so-called (p,q)-torus knots represent a class of knots which live on the surface of the solid torus $\mathbf{T}$. These knots are classified by the integers p and q, which have the property that they will always be relatively prime (i.e., their greatest common divisor is 1) [1], [10]. The integer p corresponds to how many times the knot wraps around the torus in the longitudinal direction while the integer q indicates the number of times it wraps around the torus in the meridional direction. It can be shown that the curves described by

$$x = (a + b\cos(\psi + qs))\cos(ps) \tag{2a}$$

$$y = (a + b\cos(\psi + qs))\sin(ps) \tag{2b}$$

$$z = b\sin(\psi + qs) \tag{2c}$$

represent the family of (p,q)-torus knots, which reside on the surface of $\mathbf{T}$ provided $0 \leq s \leq 2\pi$ [5]. Two views of the $(2,3)$-torus knot are shown in Fig. 3. It can be seen from Fig. 3 that the $(2,3)$-torus knot is a trefoil. The trefoil knot traverses $\mathbf{T}$ twice longitudinally and three times meridionally. Likewise, Fig. 4 shows two views of the higher order $(3,4)$-torus knot.

Any knot that can be continuously deformed into a circular loop (standard ring) is said to be an unknot or trivial knot. For this reason, the circular loop is regarded as the canonical unknot. Several variations of trivial knots or unknots can be generated as special cases of the (p,q)-torus knots. For instance, the $(1,2)$-torus knot which is shown in Fig. 5 represents a trivial knot. The toroidal helix formed by the $(1,4)$-torus knot shown in Fig. 6 is also an interesting example of a trivial knot. Finally, we note that the canonical unknot itself may be obtained as a special limiting case of a torus knot. This fact may be demonstrated by setting $b = 0$ and $p = 1$ in (2a)–(2c).

Another important property of knots is chirality. A knot is considered chiral if it is topologically distinct from its mirror image [1], [11]. This means that no matter how the knot is

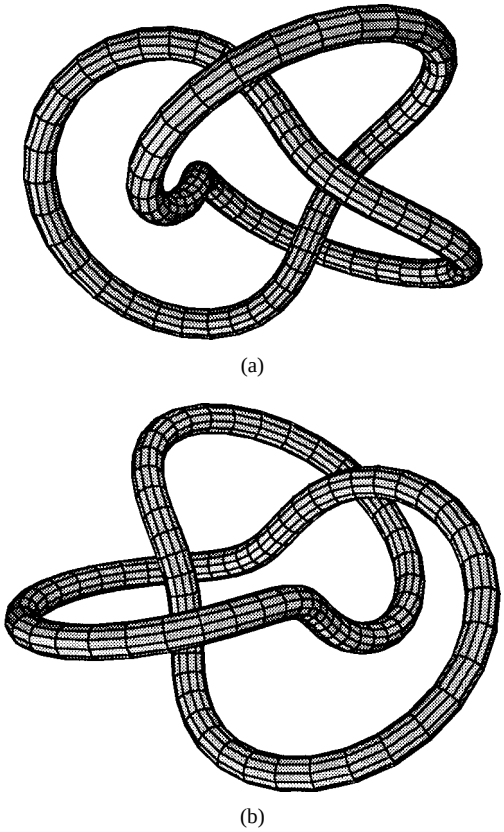

Fig. 3. Two views of a $(2,3)$-torus knot (a trefoil).

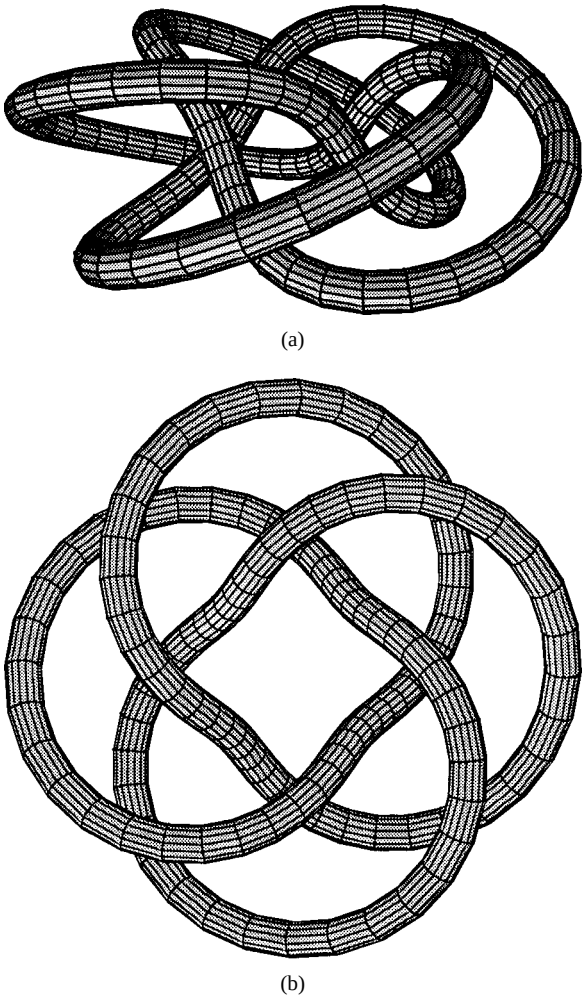

Fig. 4. Two views of a $(3,4)$-torus knot.

deformed, it cannot be superimposed on its mirror image. On the other hand, a knot that can be deformed into its mirror image is called an achiral knot. As pointed out in [7], there is a subtle distinction between the usual geometrical notion of chirality and the topological notion of chirality associated with knots. An object possesses geometrical chirality if it cannot be superimposed on its mirror image through a series of spatial translations and rotations. This definition of chirality is used in relation to inclusion geometries, such as helixes, which have been considered for chiral materials [12]. Knots which are topologically chiral, however, have the property that they cannot be superimposed on their mirror image through any kind of a continuous deformation (i.e., without breaking or cutting the knot). There are some knots, such as the figure-eight knot [11], that are geometrically chiral but topologically achiral. The $(1,2)$-torus knot and the $(1,4)$-torus knot shown in Figs. 5 and 6, respectively, are also examples of this kind of knot. The trefoil belongs to the class of knots which have both geometrical and topological chirality. In other words, the trefoil is distinct from its mirror image in the geometrical sense as well as the topological sense. This suggests that there are actually two distinct types of trefoil knots rather than just one; namely, a right-hand and a left-hand trefoil, as shown in Fig. 7. This property is also shared by the $(3,4)$-torus knot shown in Fig. 4.

2. Electromagnetic Fields of a Torus Knot

The various properties of the (p,q)-torus knots discussed above make them interesting not only from a topological point of view, but also from an electromagnetics point of view. The remainder of this section will be devoted to developing a theoretical foundation for characterizing the electromagnetic radiation and scattering properties of (p,q)-torus knots. We begin this analysis by considering the vector potential for an arbitrarily shaped wire with an electric current $\vec{I}$, which may be expressed in the general form [13]

$$\vec{A}(x,y,z) = \frac{\mu}{4\pi}\int_C \vec{I}(x',y',z')\frac{e^{-j\beta R}}{R}\,d\ell' \tag{3a}$$

where

$$R = \sqrt{(x-x')^2+(y-y')^2+(z-z')^2}. \tag{3b}$$

Vector potential expressions which are specialized for the class of (p,q)-torus knots may be derived form (3) by making use of the parameterizations introduced in (2). By representing these parameterizations in terms of the source coordinates, we have

$$x' = (a+b\cos(\psi+qs'))\cos(ps') \tag{4a}$$

$$y' = (a+b\cos(\psi+qs'))\sin(ps') \tag{4b}$$

$$z' = b\sin(\psi+qs'). \tag{4c}$$

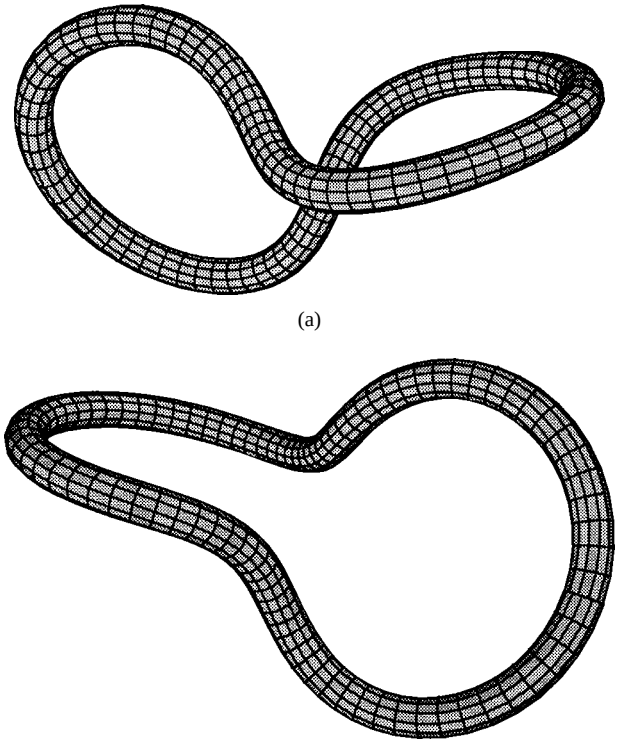

(a) (b)

Fig. 5. Two views of a $(1,2)$-torus knot (a trivial knot).

It may be shown using (4) that the incremental element of length for a (p,q)-torus knot is

$$d\ell' = \sqrt{(qb)^2 + p^2(a + b\cos(\psi + qs'))^2}\, ds' \tag{5a}$$

which, when integrated over the knot, leads to the following useful formula for arclength L:

$$L = 2\int_0^{\pi} \sqrt{(qb)^2 + p^2(a + b\cos u)^2}\, du. \tag{5b}$$

Substituting (5a) into (3a) results in an expression for the vector potential of a (p,q)-torus knot which is given by

$$\vec{A}(x,y,z) = \frac{\mu}{4\pi}\int_0^{2\pi} \vec{I}(s')\sqrt{(qb)^2 + p^2(a + b\cos(\psi + qs'))^2} \times \frac{e^{-j\beta R}}{R}\, ds'. \tag{6}$$

Furthermore, the knot current $\vec{I}$ has the general form of

$$\vec{I}(s') = I_x(s')\hat{x} + I_y(s')\hat{y} + I_z(s')\hat{z} \tag{7}$$

which implies that (6) may be separated into the following three scalar components:

$$A_x(x,y,z) = \frac{\mu}{4\pi}\int_0^{2\pi} I_x(s')\sqrt{(qb)^2 + p^2(a + b\cos(\psi + qs'))^2} \times \frac{e^{-j\beta R}}{R}\, ds' \tag{8a}$$

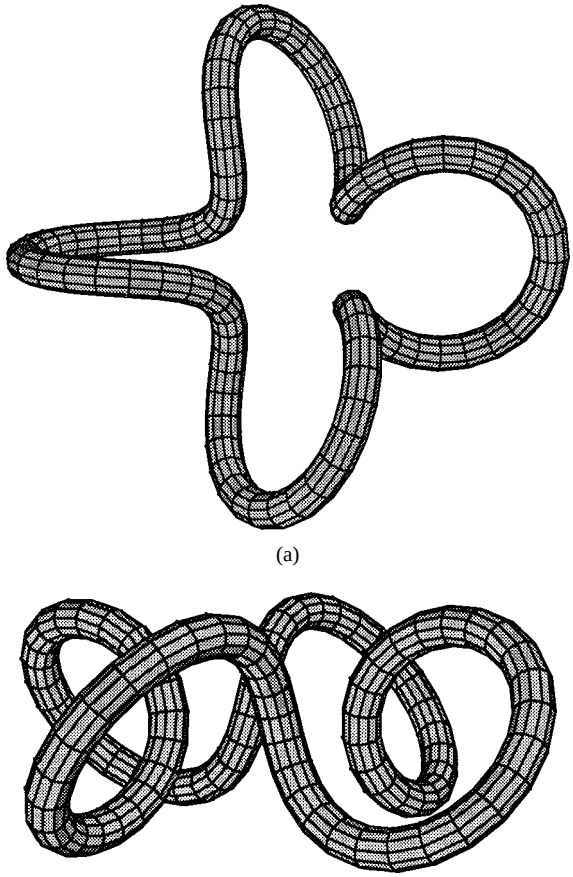

(a) (b)

Fig. 6. Two views of a $(1,4)$-torus knot (a toroidal helix).

$$A_y(x,y,z) = \frac{\mu}{4\pi}\int_0^{2\pi} I_y(s')\sqrt{(qb)^2 + p^2(a + b\cos(\psi + qs'))^2} \times \frac{e^{-j\beta R}}{R}\, ds' \tag{8b}$$

$$A_z(x,y,z) = \frac{\mu}{4\pi}\int_0^{2\pi} I_z(s')\sqrt{(qb)^2 + p^2(a + b\cos(\psi + qs'))^2} \times \frac{e^{-j\beta R}}{R}\, ds'. \tag{8c}$$

Now suppose that $I_s(s')$ represents the current distribution on the surface of a particular thin knotted wire. Then it can be shown that

$$I_x(s') = I_s(s')T_x(s') \tag{9a}$$

$$I_y(s') = I_s(s')T_y(s') \tag{9b}$$

$$I_z(s') = I_s(s')T_z(s') \tag{9c}$$

where (10a)–(10c), shown at the bottom of the next page, are the x, y and z components of the unit vector $\hat{T}$ tangent to the curve of the knot. Substituting (9a)–(9c) and (10a)–(10c) into

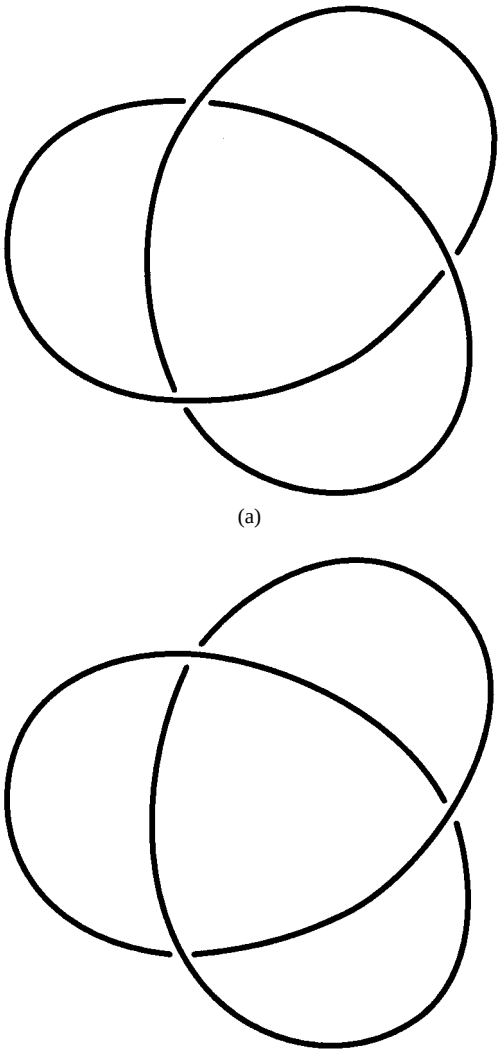

(a) (b)

Fig. 7. Two types of trefoil knots. (a) A left-hand trefoil. (b) A right-hand trefoil.

(8a)–(8c), respectively, yields

$$A_x(x,y,z) = -\frac{\mu}{4\pi}p\int_0^{2\pi} I_s(s')(a+b\cos(\psi+qs')) \times \sin(ps')\frac{e^{-j\beta R}}{R}\,ds' - \frac{\mu}{4\pi}qb\int_0^{2\pi} I_s(s')\sin(\psi+qs')\cos(ps')\frac{e^{-j\beta R}}{R}\,ds' \tag{11a}$$

$$A_y(x,y,z) = \frac{\mu}{4\pi}p\int_0^{2\pi} I_s(s')(a+b\cos(\psi+qs')) \times \cos(ps')\frac{e^{-j\beta R}}{R}\,ds' - \frac{\mu}{4\pi}qb\int_0^{2\pi} I_s(s')\sin(\psi+qs')\sin(ps')\frac{e^{-j\beta R}}{R}\,ds' \tag{11b}$$

$$A_z(x,y,z) = \frac{\mu}{4\pi}qb\int_0^{2\pi} I_s(s')\cos(\psi+qs')\frac{e^{-j\beta R}}{R}\,ds'. \tag{11c}$$

Transforming (11a)–(11c) to spherical coordinates leads to

$$A_r(r,\theta,\phi) = \frac{\mu\sin\theta}{4\pi}\left\{p\int_0^{2\pi} I_s(s')(a+b\cos(\psi+qs')) \times \sin(\phi-ps')\frac{e^{-j\beta R}}{R}\,ds' - qb\int_0^{2\pi} I_s(s')\sin(\psi+qs')\cos(\phi-ps')\frac{e^{-j\beta R}}{R}\,ds'\right\} + \frac{\mu\cos\theta}{4\pi}\left\{qb\int_0^{2\pi} I_s(s')\cos(\psi+qs')\frac{e^{-j\beta R}}{R}\,ds'\right\} \tag{12a}$$

$$A_\theta(r,\theta,\phi) = \frac{\mu\cos\theta}{4\pi}\left\{p\int_0^{2\pi} I_s(s')(a+b\cos(\psi+qs')) \times \sin(\phi-ps')\frac{e^{-j\beta R}}{R}\,ds' - qb\int_0^{2\pi} I_s(s')\sin(\psi+qs')\cos(\phi-ps')\frac{e^{-j\beta R}}{R}\,ds'\right\} - \frac{\mu\sin\theta}{4\pi}\left\{qb\int_0^{2\pi} I_s(s')\cos(\psi+qs')\frac{e^{-j\beta R}}{R}\,ds'\right\} \tag{12b}$$

$$A_\phi(r,\theta,\phi) = \frac{\mu}{4\pi}p\int_0^{2\pi} I_s(s')(a+b\cos(\psi+qs')) \times \cos(\phi-ps')\frac{e^{-j\beta R}}{R}\,ds' + \frac{\mu}{4\pi}qb\int_0^{2\pi} I_s(s')\sin(\psi+qs')\sin(\phi-ps')\frac{e^{-j\beta R}}{R}\,ds'. \tag{12c}$$

$$T_x(s') = \frac{-p(a+b\cos(\psi+qs'))\sin(ps') - qb\sin(\psi+qs')\cos(ps')}{\sqrt{(qb)^2+p^2(a+b\cos(\psi+qs'))^2}} \tag{10a}$$

$$T_y(s') = \frac{p(a+b\cos(\psi+qs'))\cos(ps') - qb\sin(\psi+qs')\sin(ps')}{\sqrt{(qb)^2+p^2(a+b\cos(\psi+qs'))^2}} \tag{10b}$$

$$T_z(s') = \frac{qb\cos(\psi+qs')}{\sqrt{(qb)^2+p^2(a+b\cos(\psi+qs'))^2}} \tag{10c}$$

Finally, general electromagnetic field expressions for the class of (p,q)-torus knots may be obtained directly from the vector potential components given in (12a)–(12c) by using the following identities:

$$\vec{E} = \frac{1}{j\omega\mu\varepsilon}[\vec{\nabla}(\vec{\nabla}\cdot\vec{A}) + \beta^2\vec{A}] \tag{13a}$$

$$\vec{H} = \frac{1}{\mu}[\vec{\nabla}\times\vec{A}]. \tag{13b}$$

We next turn our attention to the derivation of appropriate far-zone representations for the electromagnetic fields produced by a (p,q)-torus knot. It is well known that in the far-zone, simplified relationships exist between the resultant electromagnetic fields and their associated vector potential. These relationships for the fields are given below in component form [13]:

$$E_r \approx 0 \tag{14a}$$

$$E_\theta \approx -j\omega A_\theta \tag{14b}$$

$$E_\phi \approx -j\omega A_\phi \tag{14c}$$

$$H_r \approx 0 \tag{14d}$$

$$H_\theta \approx j\frac{\omega}{\eta}A_\phi = -\frac{E_\phi}{\eta} \tag{14e}$$

$$H_\phi \approx -j\frac{\omega}{\eta}A_\theta = \frac{E_\theta}{\eta}. \tag{14f}$$

Hence, in order to complete the derivation, it is only necessary to find far-zone approximations for the vector potential components A_θ and A_ϕ given in (12b) and (12c) respectively. In the far-zone, it can be shown that

$$\frac{e^{-j\beta R}}{R} \approx \frac{e^{-j\beta r}}{r}e^{j\beta[x'\sin\theta\cos\phi + y'\sin\theta\sin\phi + z'\cos\theta]} \tag{15a}$$

where

$$r = \sqrt{x^2+y^2+z^2}. \tag{15b}$$

At this point in the development, the knot parameterizations introduced in (4a), (4b), and (4c) may be used to transform (15a) into

$$\frac{e^{-j\beta R}}{R} \approx \frac{e^{-j\beta r}}{r}\Gamma(s') \tag{16a}$$

where

$$\Gamma(s') = e^{j\beta[(a+b\cos(\psi+qs'))\cos(\phi-ps')\sin\theta + b\sin(\psi+qs')\cos\theta]}. \tag{16b}$$

Substituting (16) into (12b) and (12c) leads to the required far-zone representations for A_θ and A_ϕ, which are given by

$$\begin{aligned} A_\theta(r,\theta,\phi) &\approx \frac{\mu\cos\theta}{4\pi}\frac{e^{-j\beta r}}{r}\left\{p\int_0^{2\pi} I_s(s')(a+b\cos(\psi+qs')) \right. \\ &\quad \times \sin(\phi-ps')\Gamma(s')\,ds' \\ &\quad \left. - qb\int_0^{2\pi} I_s(s')\sin(\psi+qs')\cos(\phi-ps')\Gamma(s')\,ds'\right\} \\ &\quad - \frac{\mu\sin\theta}{4\pi}\frac{e^{-j\beta r}}{r}\left\{qb\int_0^{2\pi} I_s(s')\cos(\psi+qs')\Gamma(s')\,ds'\right\} \end{aligned} \tag{17a}$$

$$\begin{aligned} A_\phi(r,\theta,\phi) &\approx \frac{\mu}{4\pi}\frac{e^{-j\beta r}}{r}p\int_0^{2\pi} I_s(s')(a+b\cos(\psi+qs')) \\ &\quad \times \cos(\phi-ps')\Gamma(s')\,ds' \\ &\quad + \frac{\mu}{4\pi}\frac{e^{-j\beta r}}{r}qb\int_0^{2\pi} I_s(s')\sin(\psi+qs') \\ &\quad \times \sin(\phi-ps')\Gamma(s')\,ds'. \end{aligned} \tag{17b}$$

C. The Torus Knot EFIE

The derivation of an EFIE for perfectly conducting knotted wires is outlined in this section. This derivation is specifically tailored to the development of an EFIE suitable for analyzing closed loops of thin wire bent in the shape of (p,q)-torus knots. A convenient place to start this development is with the general form of the EFIE for an arbitrarily curved wire [14], [15]

$$\begin{aligned} &\int_C I(\ell')\left[\frac{\partial^2}{\partial\ell\partial\ell'}G(\ell,\ell') - \beta^2\hat{\ell}\cdot\hat{\ell}'G(\ell,\ell')\right]d\ell' \\ &\quad = j\omega\varepsilon\hat{\ell}\cdot\vec{E}^i(\ell), \quad \ell\in C \end{aligned} \tag{18}$$

where $\vec{E}^i(\ell)$ represents the incident or impressed electric field and

$$G(\ell,\ell') = \frac{e^{-j\beta|\vec{r}-\vec{r}'|}}{4\pi|\vec{r}-\vec{r}'|} \tag{19}$$

is the free-space Green's function. Now suppose we define the source-point coordinates of any (p,q)-torus knot to be

$$x' = (a+b'\cos(\psi+qs'))\cos(ps') \tag{20a}$$

$$y' = (a+b'\cos(\psi+qs'))\sin(ps') \tag{20b}$$

$$z' = b'\sin(\psi+qs') \tag{20c}$$

with the corresponding field-point coordinates defined as

$$x = (a+b\cos(\psi+qs))\cos(ps) \tag{21a}$$

$$y = (a+b\cos(\psi+qs))\sin(ps) \tag{21b}$$

$$z = b\sin(\psi+qs). \tag{21c}$$

The set of knot parameterizations given in (20) and (21) may be used to obtain expressions for the unit vectors, which are tangent to the curve of these knots. A useful form of these expressions was found to be

$$\hat{\ell} = \hat{T} = \frac{\vec{V}}{|\vec{V}|} \tag{22a}$$

$$\hat{\ell}' = \hat{T}' = \frac{\vec{V}'}{|\vec{V}'|} \tag{22b}$$

where

$$\vec{V} = \frac{d\vec{r}}{ds} = V_x\hat{x} + V_y\hat{y} + V_z\hat{z} \tag{22c}$$

$$\vec{V}' = \frac{d\vec{r}'}{ds'} = V_x'\hat{x} + V_y'\hat{y} + V_z'\hat{z} \tag{22d}$$

$$V_x = \frac{dx}{ds} = -p(a + b\cos(\psi + qs))\sin(ps) - qb\sin(\psi + qs)\cos(ps) \tag{22e}$$

$$V_y = \frac{dy}{ds} = p(a + b\cos(\psi + qs))\cos(ps) - qb\sin(\psi + qs)\sin(ps) \tag{22f}$$

$$V_z = \frac{dz}{ds} = qb\cos(\psi + qs) \tag{22g}$$

$$V_x' = \frac{dx'}{ds'} = -p(a + b'\cos(\psi + qs'))\sin(ps') - qb'\sin(\psi + qs')\cos(ps') \tag{22h}$$

$$V_y' = \frac{dy'}{ds'} = p(a + b'\cos(\psi + qs'))\cos(ps') - qb'\sin(\psi + qs')\sin(ps') \tag{22i}$$

$$V_z' = \frac{dz'}{ds'} = qb'\cos(\psi + qs') \tag{22j}$$

$$|\vec{V}| = \left|\frac{d\vec{r}}{ds}\right| = \sqrt{(qb)^2 + p^2(a + b\cos(\psi + qs))^2} \tag{22k}$$

$$|\vec{V}'| = \left|\frac{d\vec{r}'}{ds'}\right| = \sqrt{(qb')^2 + p^2(a + b'\cos(\psi + qs'))^2}. \tag{22l}$$

Equations (20) and (21) may also be used to prove that the following relationship holds for (p, q)-torus knots:

$$\frac{\partial}{\partial\ell}\frac{\partial}{\partial\ell'}G(\ell, \ell') = \frac{\partial s}{\partial\ell}\frac{\partial s'}{\partial\ell'}\frac{\partial}{\partial s}\frac{\partial}{\partial s'}G(s, s') \tag{23a}$$

where

$$\frac{\partial s}{\partial\ell} = \frac{1}{|\vec{V}|} = \frac{1}{\sqrt{(qb)^2 + p^2(a + b\cos(\psi + qs))^2}} \tag{23b}$$

$$\frac{\partial s'}{\partial\ell'} = \frac{1}{|\vec{V}'|} = \frac{1}{\sqrt{(qb')^2 + p^2(a + b'\cos(\psi + qs'))^2}} \tag{23c}$$

$$G(s, s') = \frac{e^{-j\beta R}}{4\pi R} \tag{23d}$$

$$R = |\vec{R}| = |\vec{r} - \vec{r}'| = \sqrt{(x - x')^2 + (y - y')^2 + (z - z')^2} \tag{23e}$$

$$\vec{R} = R_x\hat{x} + R_y\hat{y} + R_z\hat{z} \tag{23f}$$

$$R_x = (a + b\cos(\psi + qs))\cos(ps) - (a + b'\cos(\psi + qs'))\cos(ps') \tag{23g}$$

$$R_y = (a + b\cos(\psi + qs))\sin(ps) - (a + b'\cos(\psi + qs'))\sin(ps') \tag{23h}$$

$$R_z = b\sin(\psi + qs) - b'\sin(\psi + qs'). \tag{23i}$$

Substituting (22a)–(22b) and (23a)–(23c) into (18) results in an EFIE of the form

$$\int_0^{2\pi} I_s(s')K(s, s')\,ds' = j\omega\varepsilon\vec{V}(s)\cdot\vec{E}^i(s), \quad s \in [0, 2\pi] \tag{24a}$$

where $I_s(s')$ represents the current distribution on the surface of a particular (p, q)-torus knot and

$$K(s, s') = \left[\frac{\partial}{\partial s}\frac{\partial}{\partial s'} - \beta^2\vec{V}(s)\cdot\vec{V}'(s')\right]G(s, s') \tag{24b}$$

is the kernel of the integral equation. It is possible to further simplify the EFIE given in (24) by evaluating the derivatives which appear in the expression for the kernel (24b). This leads to the result

$$\int_0^{2\pi} I_s(s')\tilde{K}(s, s')\,ds' = \frac{j}{\eta}\vec{V}(s)\cdot\vec{E}^i(s), \quad s \in [0, 2\pi] \tag{25a}$$

where

$$\tilde{K}(s, s') = \frac{1}{\beta}K(s, s') = \{(\beta R)^2[(1 + j\beta R) - (\beta R)^2]F_1(s, s') - [3(1 + j\beta R) - (\beta R)^2]F_2(s, s')\}\frac{e^{-j\beta R}}{4\pi(\beta R)^5} \tag{25b}$$

is a dimensionless form of the kernel in which

$$F_1(s, s') = \beta^2\vec{V}\cdot\vec{V}' = \beta^2\{V_xV_x' + V_yV_y' + V_zV_z'\} \tag{25c}$$

and

$$F_2(s, s') = (\beta^2\vec{R}\cdot\vec{V})(\beta^2\vec{R}\cdot\vec{V}') = [\beta^2\{R_xV_x + R_yV_y + R_zV_z\}] \times [\beta^2\{R_xV_x' + R_yV_y' + R_zV_z'\}]. \tag{25d}$$

The dependence upon the knot parameters of (25c) and (25d) is implicit. However, explicit representations of these equations may also be found which are given by

$$\begin{aligned} F_1(s, s') = {} & q^2(\beta b)(\beta b')\cos(\psi + qs)\cos(\psi + qs') \\ & + p^2[(\beta a) + (\beta b)\cos(\psi + qs)] \\ & \times [(\beta a) + (\beta b')\cos(\psi + qs')]\cos[p(s - s')] \\ & + pq(\beta b')[(\beta a) + (\beta b)\cos(\psi + qs)] \\ & \times \sin(\psi + qs')\sin[p(s - s')] \\ & - pq(\beta b)[(\beta a) + (\beta b')\cos(\psi + qs')] \\ & \times \sin(\psi + qs)\sin[p(s - s')] \\ & + q^2(\beta b)(\beta b')\sin(\psi + qs) \\ & \times \sin(\psi + qs')\cos[p(s - s')] \end{aligned} \tag{26a}$$

$$
\begin{aligned}
F_2(s,s') &= \{p[(\beta a)+(\beta b)\cos(\psi+qs)] \\
&\quad \times [(\beta a)+(\beta b')\cos(\psi+qs')]\sin[p(s-s')] \\
&\quad - q(\beta b')[(\beta a)+(\beta b)\cos(\psi+qs)] \\
&\quad \times \sin(\psi+qs')\cos[p(s-s')] \\
&\quad + q(\beta a)(\beta b')\sin(\psi+qs') + q(\beta b)(\beta b') \\
&\quad \times \sin(\psi+qs)\cos(\psi+qs')\} \\
&\quad \times \{p[(\beta a)+(\beta b)\cos(\psi+qs)] \\
&\quad \times [(\beta a)+(\beta b')\cos(\psi+qs')]\sin[p(s-s')] \\
&\quad + q(\beta b)[(\beta a)+(\beta b')\cos(\psi+qs')] \\
&\quad \times \sin(\psi+qs)\cos[p(s-s')] \\
&\quad - q(\beta a)(\beta b)\sin(\psi+qs) - q(\beta b)(\beta b') \\
&\quad \times \cos(\psi+qs)\sin(\psi+qs')\}. \qquad (26b)
\end{aligned}
$$

Finally, by using (23e) together with (20a)–(20c) and (21a)–(21c), the remarkable fact that

$$R|_{s=s'} = |b-b'| \qquad (27)$$

can easily be shown. This suggests that the knotted wire kernel (25b) will be nonsingular provided $b \neq b'$. A useful interpretation of the quantity $|b-b'|$ found in (27) is that it represents the radius of the wire used to construct the knotted antenna or scatterer. Therefore, numerical solution of the EFIE given in (25a) should yield accurate results for thin wire torus knots which satisfy the condition $|b-b'| \leq 0.01\lambda$.

The availability of the EFIE derived here is important for several reasons including the fact that it provides the basis for the development of accurate computational electromagnetics modeling techniques for knotted wires. Conventional method of moments (MoM) techniques generally approximate curved wires by a series of piecewise-linear wires, which can lead to inaccuracies in the modeling results, especially for wires which are highly looped or knotted. This new EFIE provides an alternative to the traditional approaches by allowing a MoM formulation to be developed, which is specifically tailored to the analysis of knotted wires. More accurate results could be obtained, for instance, by solving the knotted wire EFIE using either an entire domain or a curved basis function subdomain MoM formulation.

III. Special Cases

A. Small Knot Approximation

Simple closed-form expressions are derived in this section for the far-zone electromagnetic fields of electrically small torus knots. Suppose we let $b = \alpha a$ where $0 \leq \alpha \leq \frac{1}{2}$, then we may write (16b) as

$$\Gamma(s') = e^{j\beta a[(1+\alpha\cos(\psi+qs'))\cos(\phi-ps')\sin\theta+\alpha\sin(\psi+qs')\cos\theta]}. \qquad (28)$$

For sufficiently small values of a, (28) may be approximated by

$$
\begin{aligned}
\Gamma(s') &\approx 1 + j\beta a(1+\alpha\cos(\psi+qs'))\cos(\phi-ps')\sin\theta \\
&\quad + j\beta a\alpha\sin(\psi+ps')\cos\theta. \qquad (29)
\end{aligned}
$$

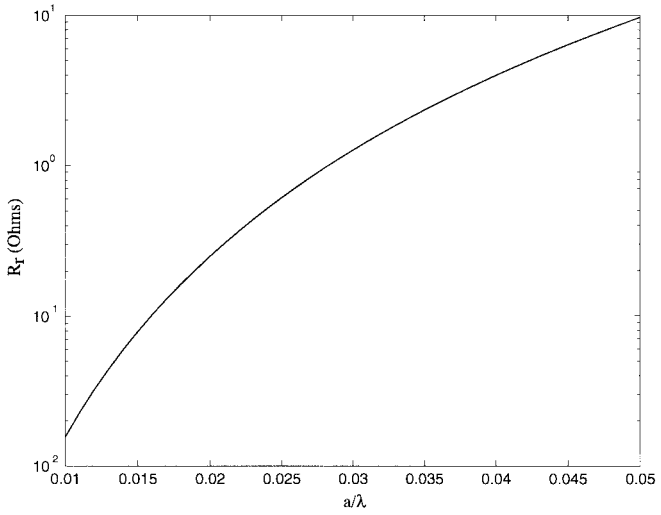

Fig. 8. The radiation resistance versus radius for an electrically small trefoil knot antenna.

The current distribution on an electrically small torus knot may be assumed to be uniform, i.e. $I_s(s') = I_0$ where I_0 is constant. Hence, under these conditions, the far-zone expressions for A_θ and A_ϕ given in (17a) and (17b), respectively, reduce to

$$
\begin{aligned}
&A_\theta(r,\theta,\phi) \\
&\quad \approx \frac{\mu a I_0\cos\theta e^{-j\beta r}}{4\pi}\frac{}{r}\left\{p\int_0^{2\pi}(1+\alpha\cos(\psi+qs'))\right. \\
&\quad \times \sin(\phi-ps')\Gamma(s')\,ds' \\
&\quad \left. - q\alpha\int_0^{2\pi}\sin(\psi+qs')\cos(\phi-ps')\Gamma(s')\,ds'\right\} \\
&\quad - \frac{\mu a I_0\sin\theta e^{-j\beta r}}{4\pi}\frac{}{r}\left\{q\alpha\int_0^{2\pi}\cos(\psi+qs')\Gamma(s')ds'\right\} \qquad (30a)
\end{aligned}
$$

$$
\begin{aligned}
&A_\phi(r,\theta,\phi) \\
&\quad \approx \frac{\mu a I_0}{4\pi}\frac{e^{-j\beta r}}{r}p\int_0^{2\pi}(1+\alpha\cos(\psi+qs')) \\
&\quad \times \cos(\phi-ps')\Gamma(s')\,ds' \\
&\quad + \frac{\mu a I_0}{4\pi}\frac{e^{-j\beta r}}{r}q\alpha\int_0^{2\pi}\sin(\psi+qs')\sin(\phi-ps')\Gamma(s')\,ds'. \qquad (30b)
\end{aligned}
$$

Next, by substituting (29) into (30) and performing the required integration, we arrive at the following closed-form small-knot approximations:

$$A_\theta \approx 0 \qquad (31a)$$

$$A_\phi \approx \frac{j\mu\beta I_0\sin\theta}{4}p\left[a^2+\frac{b^2}{2}\right]\frac{e^{-j\beta r}}{r} \qquad (31b)$$

which are valid provided $p \neq q$ and $p \neq 2q$. We note here that for the electrically small knot, A_ϕ does not depend on the parameter q. However, if higher order terms are considered in the expansion for $\Gamma(s')$ then the vector potential expressions that result will be valid for knots of larger size and, under these conditions, will depend on both p and q. Finally, the far-field representations for small knots associated with (31)

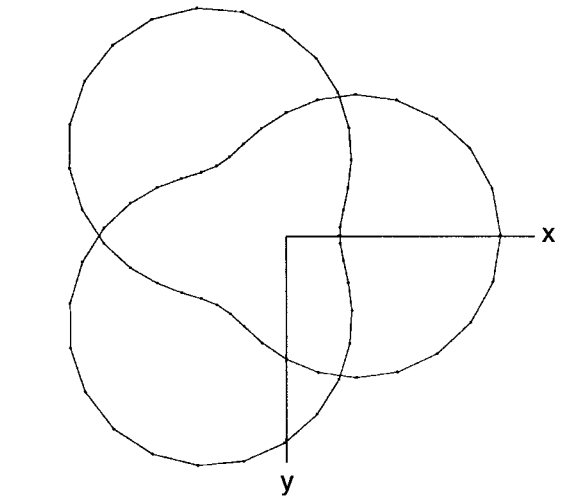

(a)

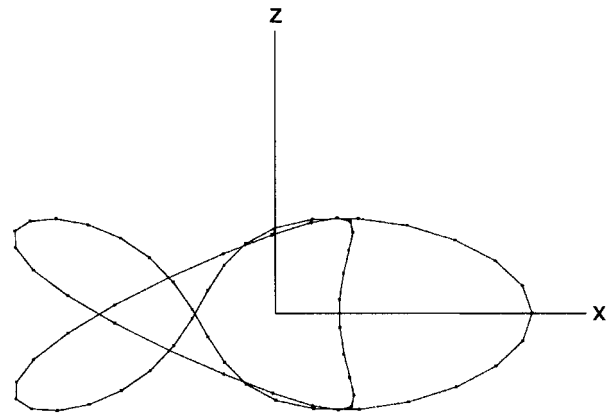

(b)

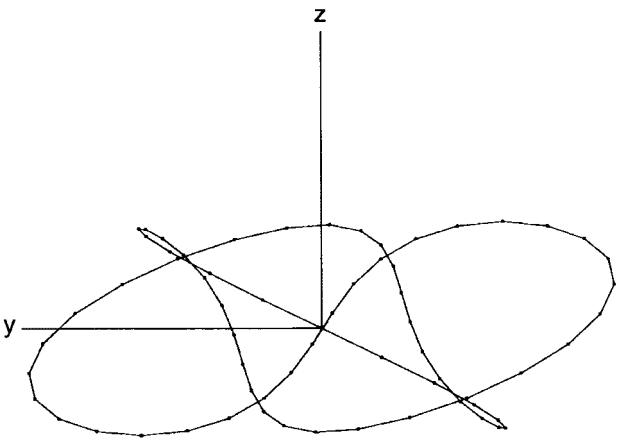

(c)

Fig. 9. (a) Top and (b), (c) side views of a thin wire model for the trefoil knot shown in Fig. 3.

may be obtained directly from (14). The resulting closed-form expressions are

$$E_r \approx 0 \tag{32a}$$

$$E_\theta \approx 0 \tag{32b}$$

$$E_\phi \approx \frac{\eta\beta^2 I_0 \sin\theta}{4} p\left[a^2 + \frac{b^2}{2}\right]\frac{e^{-j\beta r}}{r} \tag{32c}$$

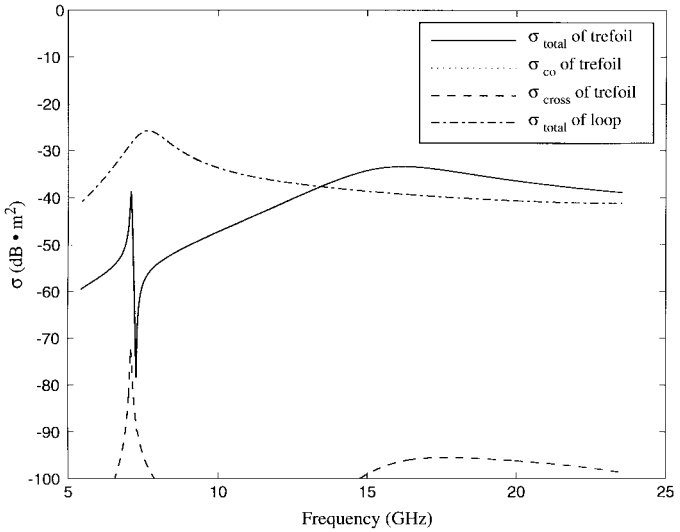

Fig. 10. Backscatter cross section versus frequency for the trefoil knot illustrated in Fig. 9(a). A linearly polarized plane wave is assumed to be incident on the knot traveling in the positive z direction with the electric field parallel to the x axis or the y axis. The backscatter cross section versus frequency for a circular loop in the x-y plane is also shown for comparison purposes.

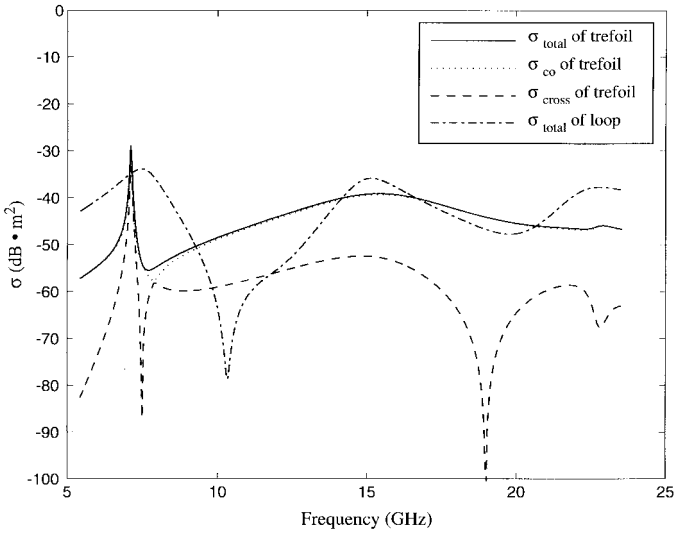

Fig. 11. Backscatter cross section versus frequency for the trefoil knot illustrated in Fig. 9(b). A linearly polarized plane wave is assumed to be incident on the knot traveling in the positive y direction with the electric field parallel to the x axis. The backscattering cross section versus frequency for a circular loop in the x-y plane is also shown for comparison purposes.

$$H_r \approx 0 \tag{32d}$$

$$H_\theta \approx -\frac{\beta^2 I_0 \sin\theta}{4} p\left[a^2 + \frac{b^2}{2}\right]\frac{e^{-j\beta r}}{r} \tag{32e}$$

$$H_\phi \approx 0 \tag{32f}$$

where $p \neq q$ and $p \neq 2q$. It is interesting to note that (32a)–(32f) are equivalent to the far-fields, which would be produced by an electrically small circular loop (canonical unknot) with an effective radius r_e and turns ratio N given by

$$r_e = \sqrt{a^2 + \frac{b^2}{2}} = a\sqrt{1 + \frac{\alpha^2}{2}} \tag{33a}$$

$$N = p. \tag{33b}$$

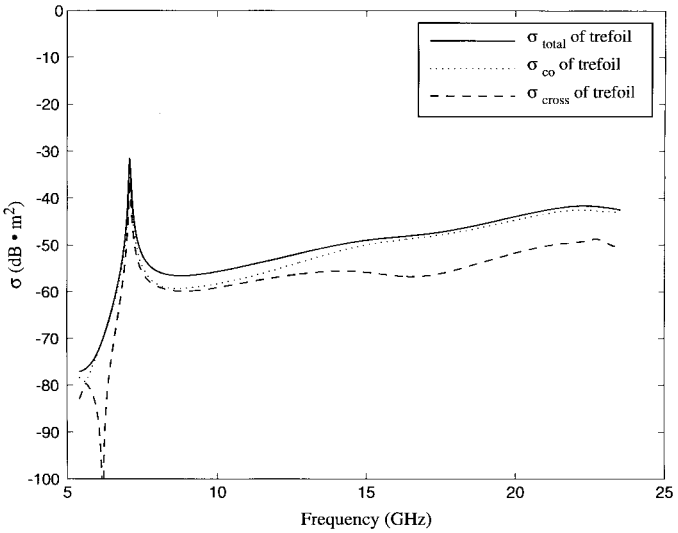

Fig. 12. Backscatter cross section versus frequency for the trefoil knot illustrated in Fig. 9(c). A linearly polarized plane wave is assumed to be incident on the knot traveling in the positive y direction with the electric field parallel to the z axis.

This also suggests that the radiation resistance for a small torus knot will have the form

$$R_r = 20\pi^2 p^2 \left[(\beta a)^2 + \frac{(\beta b)^2}{2}\right]^2 \Omega. \tag{34}$$

B. The Canonical Unknot

It was pointed out in Section II-A that the canonical unknot may be considered as a special limiting case of a torus knot. In particular, the canonical unknot is obtained as a degenerate form of a torus knot when $b = 0$ and $p = 1$. Hence, for this special case, the general vector potential expressions for the (p, q)-torus knots derived in (12a)–(12c) will reduce to

$$A_r(r,\theta,\phi) = \frac{\mu a \sin\theta}{4\pi} \int_0^{2\pi} I_s(\phi') \sin(\phi - \phi') \frac{e^{-j\beta R}}{R}\, d\phi' \tag{35a}$$

$$A_\theta(r,\theta,\phi) = \frac{\mu a \cos\theta}{4\pi} \int_0^{2\pi} I_s(\phi') \sin(\phi - \phi') \frac{e^{-j\beta R}}{R}\, d\phi' \tag{35b}$$

$$A_\phi(r,\theta,\phi) = \frac{\mu a}{4\pi} \int_0^{2\pi} I_s(\phi') \cos(\phi - \phi') \frac{e^{-j\beta R}}{R}\, d\phi' \tag{35c}$$

where

$$R = \sqrt{r^2 + a^2 - 2ar\sin\theta\cos(\phi - \phi')} \tag{35d}$$

These are, as expected, the well-known results for a circular loop antenna of radius a [16].

IV. Results

A plot of the radiation resistance as a function of radius for an electrically small trefoil knot antenna is shown in Fig. 8. This plot is based on (34) for the special case where $p = 2$ and $b = a/2$. Under these conditions, (34) reduces to the following simple formula:

$$R_r \approx 1000(\beta a)^4 \Omega. \tag{36}$$

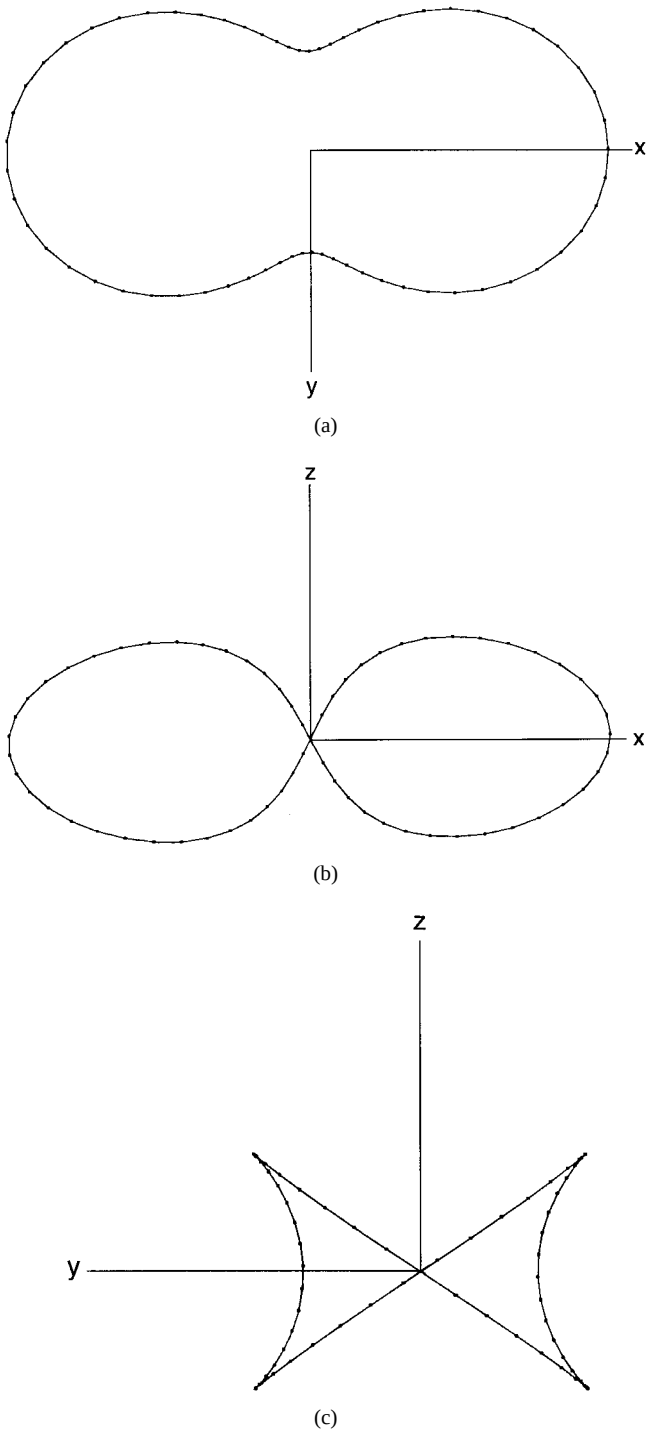

Fig. 13. (a) Top and (b), (c) side views of a thin wire model for the $(1, 2)$-torus knot shown in Fig. 5.

Fig. 8 demonstrates that a small trefoil antenna would have a relatively low value of radiation resistance. However, (33b) suggests that the radiation resistance may be increased by considering antennas, which possess a higher degree of knottedness or, more generally, a larger value of p.

Next, we turn our attention to an investigation of the scattering properties of knots. Top and side views of the trefoil shown in Fig. 3 have been included for visualization purposes in Fig. 9. The trefoil is assumed to be constructed from perfectly conducting wire with an arc length of 41.416 mm

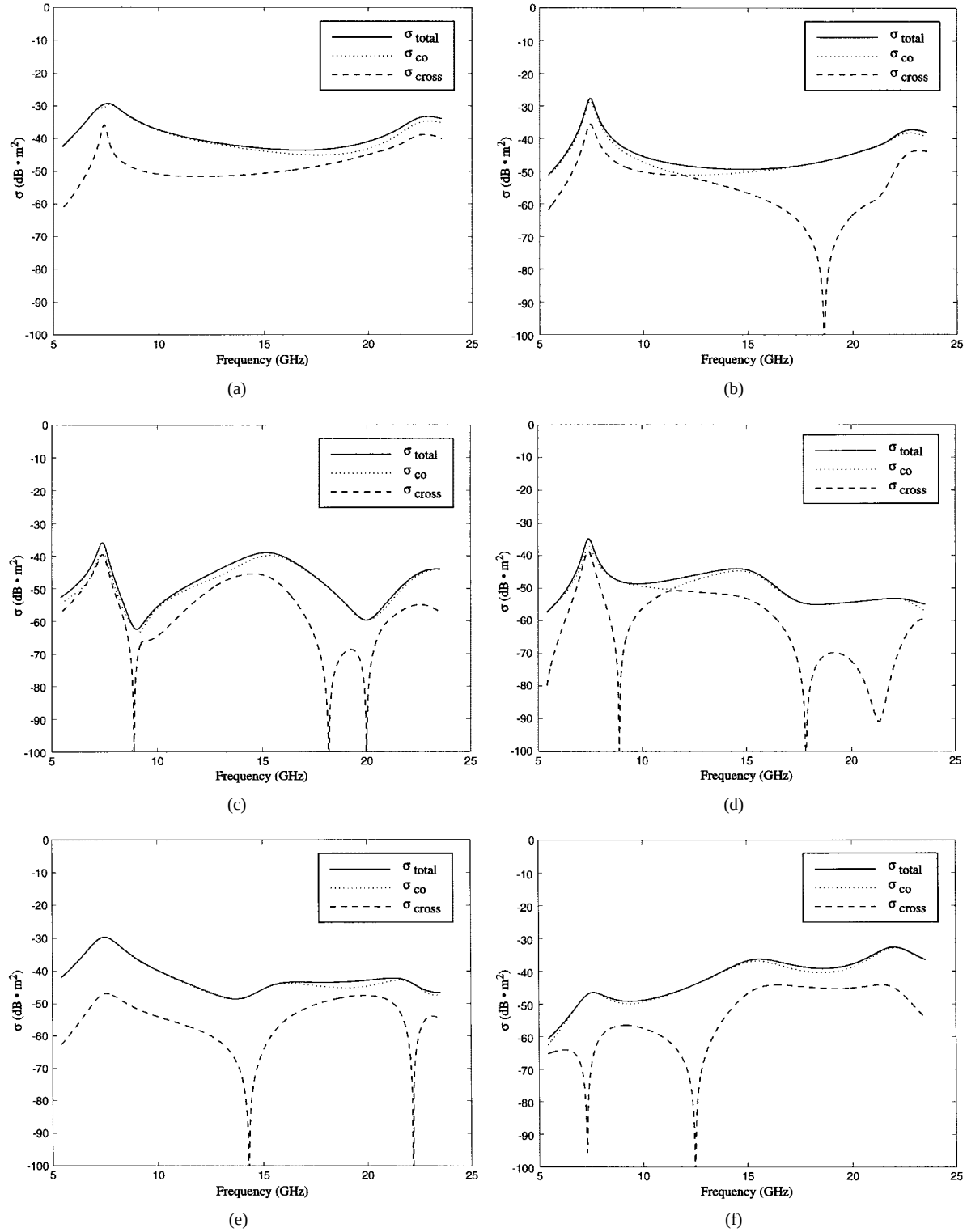

Fig. 14. Backscatter cross section versus frequency for the $(1, 2)$-torus knot illustrated in Figs. 5 and 13. A linearly polarized plane wave is assumed to be incident on the knot traveling in the: (a) positive z direction with the electric field parallel to the x-axis; (b) positive z direction with the electric field parallel to the y axis; (c) positive x-direction with the electric field parallel to the y-axis; (d) positive x direction with the electric field parallel to the z axis; (e) positive y direction with the electric field parallel to the x axis; and (f) positive y direction with the electric field parallel to the z axis.

and a radius of 5.528×10^{-2} mm. The scattering cross section of the knot may be calculated from

$$\sigma = 4\pi r^2 \frac{|\vec{E}^s|^2}{|\vec{E}^i|^2} \tag{37}$$

where $\vec{E}^i$ and $\vec{E}^s$ represent the incident and scattered electric fields, respectively [17]. A linearly polarized plane wave with an intensity of 1 V/m is assumed to be incident on the knot. The corresponding scattered field is determined using a numerical analysis procedure based on the method

of moments. This approach is followed in order to calculate the backscatter cross section as a function of frequency for a particular knot using (37).

Fig. 10 shows a plot of the backscatter cross section versus frequency for the trefoil knot illustrated in Figs. 3 and 9. The frequency range chosen for this example is between 5 GHz and 25 GHz. The curves of backscattering cross section shown in Fig. 10 were produced by an incident linearly polarized plane wave propagating along the positive z direction with the electric field parallel to the x axis [see Fig. 9(a)]. We note that for the trefoil an identical backscattering signature would be obtained if the electric field was parallel to the y axis rather than the x axis. The solid curve shown in Fig. 10 represents the total backscatter cross section which is denoted by σ_{total}. The dotted and dashed curves, on the other hand, represent the copolarized backscatter cross section (σ_{co}) and the cross-polarized backscatter cross section (σ_{cross}) respectively. For the case considered in Fig. 10, the total backscatter cross section is essentially the same as the copolarized backscatter cross section.

The resonance frequencies for a (p,q)-torus knot may be estimated by using the approximate formula

$$f_n = n\left(\frac{c}{L}\right), \qquad \text{for } n = 1, 2, \cdots \tag{38}$$

where L represents the arc length of the knot as defined in (5b). Note that these are the same resonances that would be associated with a circular loop (canonical unknot) having a circumference equal to L. The trefoil knot considered in Figs. 3 and 9 has an arc length of 41.416 mm, which corresponds to one wavelength at 7.24 GHz. This fact is substantiated by (38) which suggests that the first resonance should occur at a frequency of approximately $f_1 = 7.24$ GHz. Fig. 10 demonstrates that a sharp resonance is indeed present at this frequency. However, it is interesting to note that in this case, all higher order resonances are suppressed. The backscatter cross section for a circular loop in the x–y plane with a 41.416-mm circumference ($f_1 = 7.24$ GHz) is also shown in Fig. 10 for comparison purposes. From this we see that the trefoil knot has a much sharper first resonance than does its circular loop counterpart.

Next, suppose we consider a linearly polarized plane wave, which is incident on the trefoil knot along the positive y direction with the electric field parallel to the x axis [see Fig. 9(b)]. A plot of the backscatter cross section as a function of frequency for this case is shown in Fig. 11. The backscatter cross section that would result from a circular loop of equivalent arclength contained in the x–y plane is also shown in Fig. 11. Again, we find that the first resonance of the trefoil is relatively sharp in contrast to the loop. There are also some noticeable differences in the behavior of the higher order resonance.

The last case that will be examined for the trefoil involves its response to an incident linearly polarized plane wave propagating along the y direction with the electric field parallel to the z axis [see Fig. 9(c)]. Curves of the backscatter cross section for this case are shown in Fig. 12. It is important to point out that under these circumstances, the incident field would not couple to a circular loop lying in the x–y plane. On the other hand, Fig. 12 shows evidence of significant field coupling to the trefoil. This leads to the conclusion that the trefoil knot experiences a strong field coupling for all possible polarizations and angles of incidence, whereas the circular loop does not.

A three-dimensional view of a $(1,2)$-torus knot is shown in Fig. 5. The geometry for this particular knot can be generated by pinching and twisting a circular loop. Therefore, by definition, the $(1,2)$-torus knot is an example of a trivial knot. The top and side views of this knot are shown in Fig. 13. The various curves contained in Fig. 14 document how the backscatter cross section of the $(1,2)$-torus knot depends on frequency, polarization and angle of incidence. The backscattering results shown in Fig. 14 were produced by a $(1,2)$-torus knot with a wire arc length and radius of 41.416 mm and 5.528×10^{-2} mm, respectively.

V. Conclusion

Knot electrodynamics is an emerging area of research that seeks to combine aspects of knot theory with Maxwell's theory of electromagnetism. The primary purpose of this paper has been to establish a rigorous mathematical foundation from which analysis techniques may be developed and applied toward the study of knot electrodynamics problems. This paper focuses on the particular class of knots, known as torus knots, which have interesting topological as well as electromagnetic properties. These knots derive their name from the fact that they reside on the surface of a solid torus and, consequently, useful parametric representations for them may be found. A new knotted wire EFIE was derived based on the available parameterizations for (p,q)-torus knots. These parameterizations were also used to derive expressions for the electromagnetic fields radiated by (p,q)-torus knots; including simple closed-form representations for the far-fields of electrically small knots. Finally, several examples were presented and discussed which illustrate the unique radiation and scattering properties associated with various (p,q)-torus knots.

Acknowledgment

The author would like to thank R. Mittra for his discussions concerning the backscattering properties of knots. He would also like to thank T. W. Colegrove for the assistance he provided during the course of this work.

References

[1] C. C. Adams, *The Knot Book: An Elementary Introduction to the Mathematical Theory of Knots*. New York: Freeman, 1994.
[2] S. Wasserman, J. Dungan, and N. Cozzarelli, "Discovery of a predicted DNA knot substantiates a model for site-specific recombination," *Sci.*, vol. 229, pp. 171–174, July 1985.
[3] T. Schlick and W. K. Olson, "Trefoil knotting revealed by molecular dynamics simulations of supercoiled DNA," *Sci.*, vol. 257, pp. 1110–1115, 1992.
[4] D. M. Walba, "Topological stereochemistry," *Tetrahedron*, vol. 41, no. 16, pp. 3161–3212, 1985.
[5] S. J. Lomonaco, Jr., "The modern legacies of Thomson's atomic vortex theory in classical electrodynamics," in *The Interface of Knots and*

Physics, L. H. Kauffman, Ed. Providence, RI: Amer. Math. Soc., 1996, pp. 145–166.
[6] G. E. Marsh, "Helicity and electromagnetic field topology," in *Advanced Electromagnetism: Foundations, Theory and Applications*, T. W. Barrett and D. M. Grimes, Eds. Singapore: World Scientific, 1995, pp. 52–76.
[7] O. Manuar and D. L. Jaggard, "Backscatter signatures of knots," *Opt. Lett.*, vol. 20, no. 2, pp. 115–117, Jan. 1995.
[8] D. L. Jaggard and O. Manuar, "Can one "hear" the handedness or topology of a knot?," in *Proc. IEEE Antennas Propagat. Soc. Int. Symp. URSI Radio Sci. Meet. URSI Dig.*, Newport Beach, CA, June 1995, p. 244.
[9] O. Manuar and D. L. Jaggard, "Wave interactions with trefoils and untrefoils," in *Proc. IEEE Antennas Propagat. Soc. Int. Symp. URSI Radio Sci. Meet. URSI Dig.*, Baltimore, MD, July 1996, p. 279.
[10] H. Seifert and W. Threlfall, *A Textbook of Topology*. New York: Academic, 1980.
[11] L. H. Kauffman, *Knots and Physics*. Singapore: World Scientific, 1991.
[12] D. L. Jaggard, A. R. Mickelson, and C. H. Papas, "On electromagnetic waves in chiral media," *Appl. Phys.*, vol. 18, pp. 211–216, 1979.
[13] C. A. Balanis, *Antenna Theory, Analysis and Design*. New York: Wiley, 1982.
[14] K. K. Mei, "On the integral equations of thin wire antennas," *IEEE Trans. Antennas Propagat.*, vol. AP-13, pp. 374–378, May 1965.
[15] J. J. H. Wang, *Generalized Moment Methods in Electromagnetics: Foundation and Computer Solution of Integral Equations*. New York: Wiley, 1991.
[16] D. H. Werner, "An exact integration procedure for vector potentials of thin circular loop antennas," *IEEE Trans. Antennas Propagat.*, vol. 44, pp. 157–165, Feb. 1996.
[17] J. J. Bowman, T. B. A. Senior, and P. L. E. Uslenghi, *Electromagnetic and Acoustic Scattering by Simple Shapes*. New York: Hemisphere, 1987.

Douglas H. Werner (S'81–M'89–SM'94) received the B.S., M.S., and Ph.D. degrees in electrical engineering from the Pennsylvania State University, State College, in 1983, 1985, and 1989, respectively, and the M.A. degree in mathematics at the same university, in 1986.

He is an Associate Professor in the Department of Electrical Engineering, Pennsylvania State University, is a member of the Communications and Space Sciences Laboratory (CSSL), and is affiliated with the Electromagnetic Communications Laboratory. He is also a Senior Research Associate in the Intelligence and Information Operations Department of the Applied Research Laboratory. He is an Associate Editor of *Radio Science*, published numerous technical papers and proceedings articles, and is the author of three book chapters. He is currently in the process of coediting (with R. Mittra) *Frontiers in Electromagnetics* (Piscataway, NJ: IEEE Press). His research interests include theoretical and computational electromagnetics with applications to antenna theory and design, microwaves, wireless and personal communication systems, electromagnetic wave interactions with complex materials, fractal and knot electrodynamics, and genetic algorithms.

Dr. Werner was presented with the 1993 Applied Computational Electromagnetics Society (ACES) Best Paper Award and was also the recipient of a 1993 International Union of Radio Science (URSI) Young Scientist Award. In 1994 he received the Pennsylvania State University Applied Research Laboratory Outstanding Publication Award. He has also received several Letters of Commendation from the Pennsylvania State University Department of Electrical Engineering for outstanding teaching and research. He is a member of the American Geophysical Union (AGU), URSI Commissions B and G, the Applied Computational Electromagnetics Society (ACES), Eta Kappa Nu, Tau Beta Pi, and Sigma Xi.